International Journal of Modern Physics A
Vol. 36, Nos. 11 & 12 (2021) 2140015 (17 pages)

DOI: 10.1142/S0217751X21400157

A torsional thrust stand for measuring the thrust response time of micro-Newton thrusters

Chao Yang, Jian-Wu He, Li Duan* and Qi Kang†

Center for Gravitational Wave Experiment, National Microgravity Laboratory, Institute of Mechanics, Chinese Academy of Sciences (CAS), Beijing 100190, China

Taiji Laboratory for Gravitational Wave Universe (Beijing/Hangzhou), University of Chinese Academy of Sciences (UCAS), Beijing 100049, China
*duanli@imech.ac.cn
†kq@imech.ac.cn

‡*On behalf of The Taiji Scientific Collaboration*

Received 15 September 2020
Revised 16 October 2020
Accepted 30 October 2020
Published 9 April 2021

Drag-free technology functions as the keystone for space-based gravitational wave detection satellites moving along a geodesic path, like the Laser Interferometer Space Antenna (LISA) Pathfinder, to achieve ultra-high microgravity level. Several prerequisites for micro-thrusters operated under the drag-free technique include constantly adjustable thrust, high resolution, low noise and fast response time. Accordingly, a torsional thrust measurement system was methodically devised to measure the thrust response time of such micro-thrusters on the ground. The characteristics of the dynamic thrust change with time are inverted by the angular displacement of the torsional pendulum, established by the dynamic equation of the same, thus, measuring the rise/fall time of the thrust applied to the torsional pendulum. Calibration of the torsional pendulum thrust measurement system is carried out by the standard electrostatic force generated by the electrostatic comb-drive or microelectromechanical actuator, facilitating the suitable identification of the pendulum parameters. Afterwards, the electrostatic and electromagnetic forces generated by the actuator are applied to validate the measurable thrust response time of the torsional thrust stand. The experimental results show that the above-mentioned thrust stand can effectively measure the thrust response time up to 10 ms for a thrust step in 10 s of micronewtons, which qualifies as the thrust response time required by micro-thrusters for space-based gravitational wave detection.

Keywords: Gravitational waves; micro-Newton thruster; thrust measurement; thrust response time; torsional thrust stand.

*,†Corresponding authors.
‡For more details, please refer to article 2102002 of this Special Issue.

1. Introduction

The first direct observation of a gravitational wave event was achieved by the ground-based Laser Interferometer Gravitational-wave Observatory (LIGO) in 2015.[1] Consequently, this breakthrough discovery won the 2017 Nobel Prize in Physics for LIGOs three lead scientists — Rainer Weiss, Barry Barish and Kip Thorne. Space-based gravitational wave detection (GWD) is deemed to be a substantially insightful component of the multi-messenger astronomy for exploring the gravitational domain, since it can delve into a wider range of gravitational radiation sources as compared to the ground based GWD[2] and is capable of yielding considerably more information that remains directly undetectable from the ground or through electromagnetic means. The Laser Interferometer Space Antenna (LISA) mission — a joint collaboration of the European Space Agency (ESA) and the National Aeronautics and Space Administration (NASA) — started in the 1990s, has progressed into an advanced space-based gravitational wave detection program.[3,4] In December 2015, ESA successfully launched the LISA-Pathfinder, a proof-of-concept mission, to verify future key technology with a space-based observatory. The results of the first round of scientific work surpassed all expectations.[4–6] In 2008, the Space Gravitational Wave Detection Demonstration Group, initiated by the Chinese academician — Hu Wenrui from the Institute of Mechanics of the Chinese Academy of Sciences (CAS), was established and later officially named as "Taiji Program in Space", in 2012. In 2016, CAS launched a strategic priority research program aimed at the pre-study of space-based GWD.[7,8] At the end of August 2019, CAS successfully launched the satellite called "Taiji-1", meaning 'Supreme Ultimate', from the Jiu Quan Satellite Launch Center. 'Taiji-1' satellite mission is the foremost step of the "Taiji Program in Space", which aims at testing key technologies, such as high-precision and ultra-stable laser interferometer, gravitational reference sensor, ultra-high precision drag-free control and ultra-stable and ultra-static satellite platform, related to the space-based detection of gravitational waves.[9,10]

The successful launch of China's first space-based gravitational wave detection technology verification satellite — "Taiji-1", followed by the successful completion of the first phase of "Taiji-1" in-orbit test missions have laid the robust foundation for China's objective of space-based detection of gravitational waves, enabling China to be the forerunner for making breakthroughs in this intriguing research domain.[9] The radio frequency ion micro thruster (μRIT), developed by the Institute of Mechanics under the CAS, facilitated the successful execution of China's first in-orbit drag-free technology experiment conducted by "Taiji-1".[10] Certain essential conditions associated with the micro-thrusters under the drag-free technology include that the thrust be continuously adjustable from 5–50 μN and the response time be less than 50 ms (when the thrust change range is 25 μN), which proves to be a challenging endeavor for micro-thrusters in terms of measuring the thrust response time.

Several advanced thrust measurement devices have been developed for micro-thruster characterization by various space agencies such as ONERA,[11] Thales Alenia Space Italia,[12] European Space Agency,[13] Busek Company,[14] NASA Goddard Space Flight

Center,[15] George Washington University,[16] Huazhong University of Science and Technology[17] and Aerospace Engineering University.[18] These thrust measurement devices are primarily designed to measure parameters like the thrust size, thrust resolution and impulse. The background noise of some measurement devices is better than 0.1 μN/Hz$^{1/2}$ (10 mHz–1 Hz),[11,12] hence they can be utilized for noise measurement of micro-thrusters. Nevertheless, there are relatively few studies available concerning the measurement of micro-level thrust response time. A typical example is the instrument for measuring thrust and noise called "Nanobalance" designed by Thales Alenia Space Italia, which is capable of attaining up to 90% of a 36 μN commanded force step in 100 ms.[12] The instrument successfully measured the thrust response time of the LISA Pathfinder field emission thruster. The measurement results of the Pathfinder thruster illustrate that it takes about 270 ms for the thrust to progress from 0.3 μN to 30.3 μN and 170 ms to retreat from 30.3 μN to 0.3 μN.[19] However, no currently available thrust measuring device can realize up to 90% of a 25 μN commanded force step in 50 ms.

In response to the thrust calibration requirements of "Taiji-1", μRIT and the "Taiji Program" micro-thruster, the team involved in this paper designed and modeled a torsion-based micro-thrust measurement system. This study first describes the composition, measurement principle and static thrust measurement performance of this system, and then introduces the experimental research of thrust response time measurement. The measurement delay phenomenon encountered in the experiment performed is also discussed comprehensively. Finally, a conclusion is presented.

2. Thrust Measurement System

2.1. *System composition*

The micro-thrust measurement system based on the torsional pendulum is as shown in Fig. 1, which includes thrust measurement device, vacuum chamber, Micro-epsilon capaNCDT6530 capacitive displacement sensor, Mettler Toledo ME55 high-precision electronic balance, Keithley 2400 digital source meter and upper computer for managing the data. It also employs standard force generation and torsion self-calibration software, as well as a micro-thrust measurement software. The upper computer records the sensor displacement through ethernet communication. The source meter communicates with the host computer through the GPIB interface to realize high-voltage output and acquisition. The electronic balance reading is recorded in the host computer for further processing.

The torsional pendulum utilized in the thrust measuring device is connected to the pedestal installed on the optical table through a pivot. One end of the torsional pendulum is contoured with threaded holes meant for thruster installation, and the other end is designed with a fixture used for the installation of capacitive displacement sensors. The ground end of the electrostatic comb is mounted on the torsional pendulum, and the high voltage end is fixed on the three-axismotion platform. Numerous screw holes are reserved to employ the counterweight on the torsional pendulum. The permanent magnet

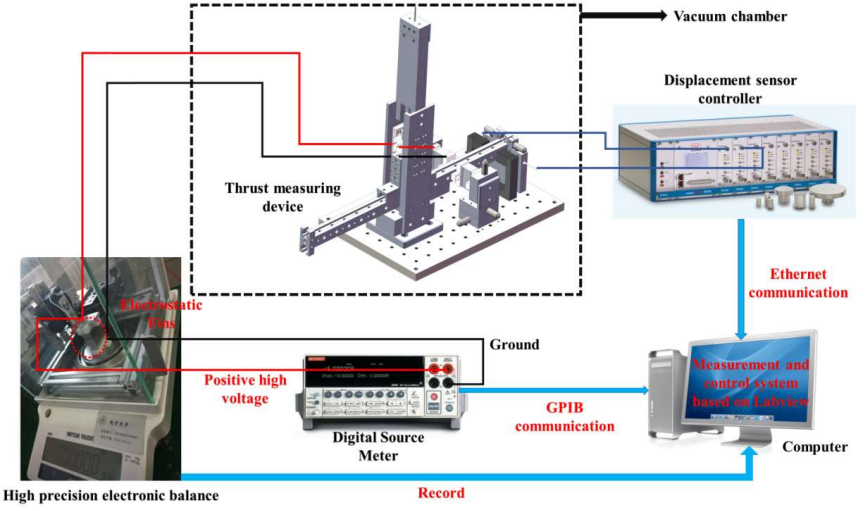

Fig. 1. Schematic of the thrust measurement system.

damping device availed in the system comprises of a U-shaped iron piece and two strong magnetic blocks, placed on the front and the rear sides of the torsional pendulum. A metal liquid box is placed directly above the pivot so as to bridge the electric wire, which aids in eliminating the torque interference induced by the wire during the actual thrust measurement.[20] Meanwhile, the gas supply tube is placed parallel to the pivot with an aim to minimize the impact of the torque generated by the tube.

2.2. *Measuring principle*

The thrust acts on the torsional pendulum guiding it into a rotation. This thrust can be measured by determining the deflection of displacement and implementing it in the dynamic equation of the torsional pendulum.

The equation of motion of the torsional pendulum can be expressed as follows:

$$J\ddot{\theta} + \lambda\dot{\theta} + k\theta = F(t)L\,, \tag{1}$$

where J denotes the moment of inertia of the torsional pendulum, θ represents the angular displacement of the torsional pendulum, λ is the damping factor, k stands for the pivot torsional coefficient and $F(t)$ and L represent the force acting on the torsional pendulum and the length of the arm, respectively.

If the torsional pendulum swings slightly, k can be considered as a constant. It appears highly challenging to measure the angular displacement of the torsional pendulum in practice since it spins on a rather small scale. The displacement sensor is utilized to determine the displacement of one end of the torsional pendulum, and is then

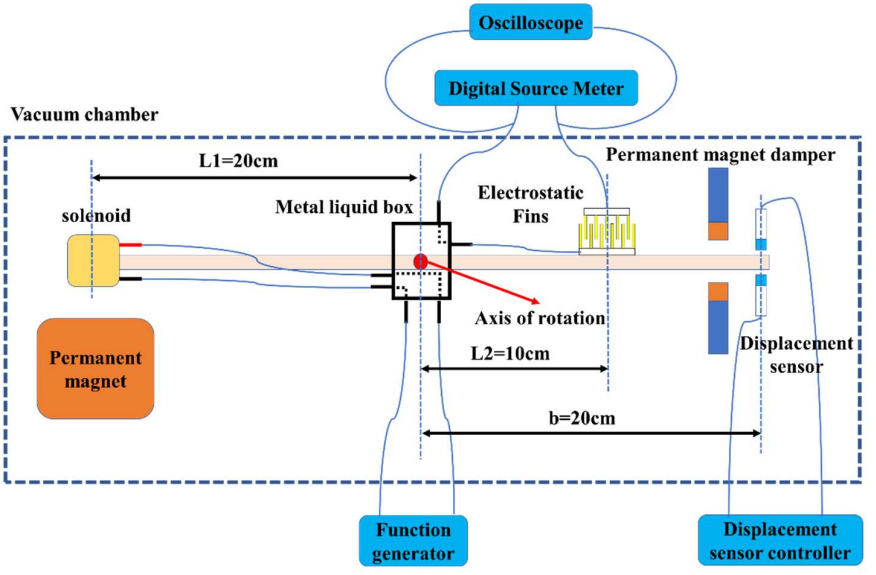

Fig. 2. Principle of the thrust measuring device.

converted into angular displacement. At a small angle:

$$\theta \approx \mathbf{tg}\,\theta = x/b\,, \tag{2}$$

where x is the displacement measured by the displacement sensor, and b denotes the length from the measuring point of the sensor to the bearing position, so Eq. (1) can be rewritten as follows:

$$J\ddot{x} + \lambda\dot{x} + kx = F(t)Lb\,. \tag{3}$$

According to Eq. (3), if the torsional pendulum system parameters such as J, λ, k are determined, the displacement x can be differentiated to obtain the velocity $\dot{x}$, and the velocity $\dot{x}$ can be further differentiated to obtain the acceleration $\ddot{x}$, thus, the dynamic thrust force can be expressed as follows:

$$F(t) = (J\ddot{x} + \lambda\dot{x} + kx)/Lb\,. \tag{4}$$

After an instantaneous excitation is applied to the suspending torsional pendulum, the system oscillates freely. By means of frequency spectrum analysis of the displacement measured by the displacement sensor, the undamped oscillation frequency f_0 and the damped oscillation frequency f of the torsional pendulum are obtained. The corresponding angular frequencies are as follows:

$$\omega_0 = 2\pi f_0\,, \tag{5}$$

$$\omega = 2\pi f\,. \tag{6}$$

Then, the moment of inertia of the torsional pendulum can be expressed as follows:

$$J = k/(2\pi f_0)^2 . \tag{7}$$

The damping factor is

$$\lambda = 2J\sqrt{(2\pi f_0)^2 - (2\pi f)^2} . \tag{8}$$

A constant force F_t acts on the torsional pendulum. If damping occurs, the torsional pendulum eventually stabilizes at a constant angle. Then, Eq. (3) becomes

$$kx = F_t Lb . \tag{9}$$

Hence, the torsional pendulum system parameters, J, λ and k, can be derived by Eqs. (7)–(9), respectively.

2.3. *Standard force calibration*

Electrostatic force devices, like electrostatic comb-drive, possess certain advantages over the traditional calibration techniques, such as involving no physical contact with the thrust stand and the ability to apply a constantly varying force as a function of voltage.[21]

The electrostatic comb-drive actuator comprises of at least two comb teeth. The electrostatic force develops a good linear relationship with the square of the input voltage in the insertion direction.[22,23]

$$F = N\varepsilon_0 V^2 (h/g), \tag{10}$$

where F denotes the electrostatic force, whose direction is parallel to the electrostatic comb teeth, N represents the number of pairs of electrostatic comb teeth, ε_0 signifies the vacuum dielectric constant, V is the positive high voltage, h is the width of the electrostatic comb and g represents the distance between the cross teeth of the electrostatic comb.

This experiment utilizes the Mettler Toledo ME55 high-precision electronic balance to calibrate the electrostatic force. The Keithley 2400 digital source meter outputs and measures the voltage between the electrostatic combs. Implementing the balance reading and Beijing's acceleration of gravity, $g = 9.8015$ N/Kg, the relationship between the quadratic voltage and the standard force is as shown in Fig. 3.

The relationship between the electrostatic force and the quadratic voltage is

$$F = q_1 + q_2 * V^2 , \tag{11}$$

where $q_1 = 0.004712\ \mu$N, $q_2 = 0.001108\ \mu\text{N}/V^2$, and the root mean square error is 0.0486.

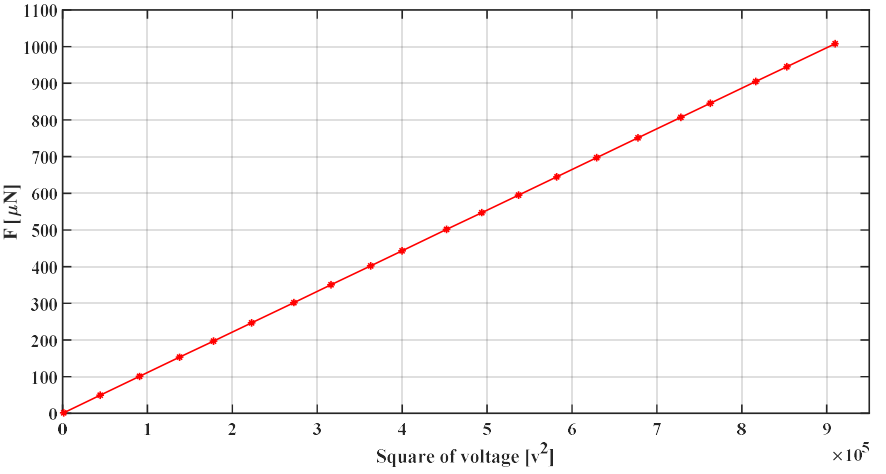

Fig. 3. The relationship between the electrostatic force and the square of the voltage.

2.4. *System resolution, measurement range and background noise*

The thrust resolution of the balance is assessed utilizing the standard force. The thrust resolution and range of the system are evaluated based on the relationship between the standard force arm L_2 and the thruster thrust arm L_1, in Fig. 2. The specific calibration method implemented can be found in Ref. 24.

The resolution calibration result is as shown in Fig. 4. The standard force commands are 0.1, 0.05 and 0.025 μN, while the displacement sensor further determines various steps. Equivalent thrust steps of 0.025 μN amplitude emerge quite striking amid the background noise, and thus, the thrust resolution of this system appears to be 0.025 μN.

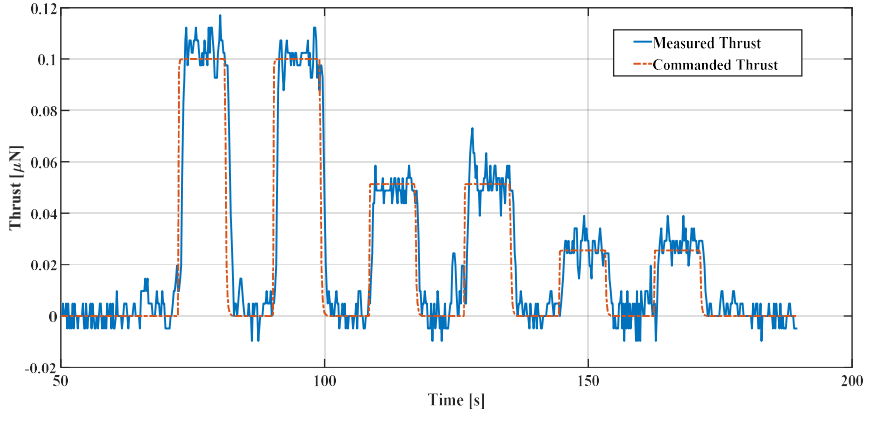

Fig. 4. (Color online) Thrust measurement system resolution — the red dotted line represents the standard force command and the blue solid line represents the measured thrust.

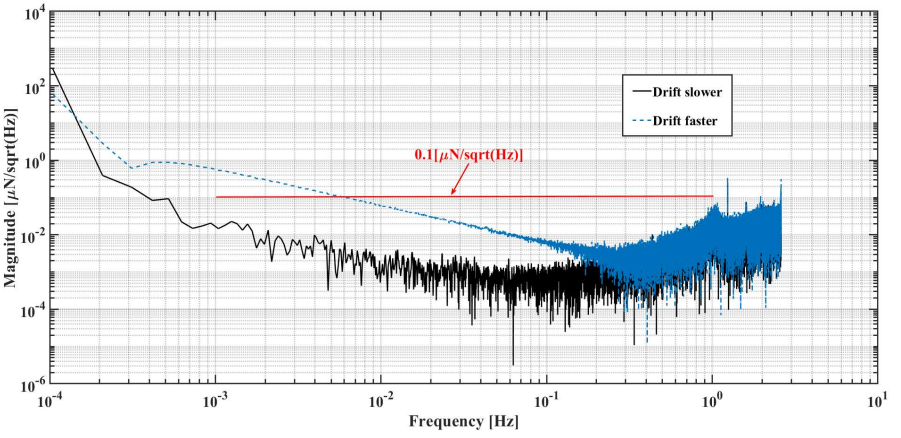

Fig. 5. PSD of the thrust measurement system with background noise.

The detailed thrust measurement range is not described in this paper. Combining the measurement results availed from Ref. 24, the thrust measurement range appears to be 0.025–400 μN.

Within the vacuum chamber, the displacement data was continuously collected and recorded for about 33 h. The temperature variation leads to a long-term drift in displacement parameter. Taking the displacement data of the time periods with faster and slower drift, converting them into thrust at the thruster installation position, and then evaluating the background noise power spectrum density, gives us the result, as shown in Fig. 5.

The background noise power spectral density of the faster drift stage performs better than $0.1\mu N/\sqrt{Hz}$ value in the 10 mHz–1 Hz frequency band, and when the drift tends to be slow, it performs better than $0.1\mu N/\sqrt{Hz}$ value in the 1 mHz–1 Hz frequency band.

3. Experimental Study of Response Rime Measurement

Before executing the experiment of response time measurement, it is essential to calibrate the system parameters of the torsional pendulum. The torsion coefficient 'k' of the system is 0.2186 N·m/rad, the moment of inertia J is 0.0053747 kg·m^2 and the damping factor is 0.00674194 N·m·s/rad.

3.1. *Standard force rise/fall time measurement*

The electrostatic comb-drive actuator remains the standard force generating device, which is equivalent to a capacitor. The capacitance level is in terms of picofarad, hence the charging time tends to be less than 1 ms. According to Eq. (10), the rise and fall time of the generated electrostatic force can primarily be determined by measuring the rise and fall time of high voltage. The true rise and fall times of the standard force can be acquired by collecting and estimating the high voltage value, and then comparing it with the

torsional pendulum measurement results to validate the accuracy of the torsional pendulum measurement system.

The digital source meter inputs a square wave having a period of 4 s to the electrostatic comb-drive. The calculated thrust curve of electrostatic force can be obtained by garnering the high voltage through an oscilloscope. At the same time, the displacement value is collected at 3906.25 Hz and then filtered. Eq. (4) is employed to acquire the electrostatic force curve, which is measured by the torsional pendulum. The result is as shown in Fig. 6.

In Fig. 6(a), the solid black line represents the displacement prior to unfiltered processing and the red dashed line represents the displacement after filtering. In Fig. 6(b), the red solid line represents the calculated thrust and the black dashed line denotes the measured thrust. Figure 6(c) demonstrates the comparison between calculated and measured thrust rise time. Figure 6(d) portrays the comparison between the calculated and the measured thrust drop time.

It can be inferred from Fig. 6 that it takes about 100 ms for the calculated thrust and 110 ms for the measured thrust to rise to 90% of the maximum thrust. However, the calculated thrust takes 210 ms while the measured thrust takes 220 ms to drop from the maximum, to 10% of the maximum thrust. The measurement result of thrust response time transpires similar to the real situation, but exhibits a measurement delay of 10 ms. The analysis of this delay is discussed in detail in Sec. 4.

3.2. *Electromagnetic force rise/fall time measurement*

Low voltage (about 2.5 V) is utilized to supply power to the electromagnetic spiral coil. The response time of the electromagnetic force generated by this coil and the permanent magnet happens to be quite fast, with a swift rise and fall time of about less than 1 ms.

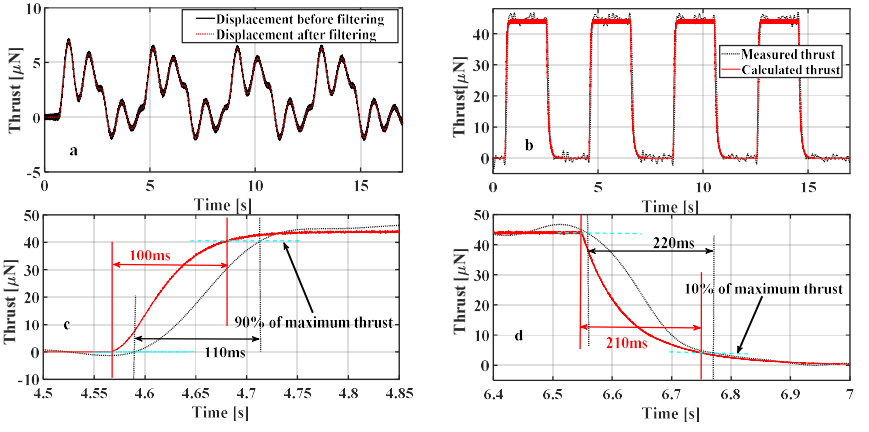

Fig. 6. Standard force response time measurement.

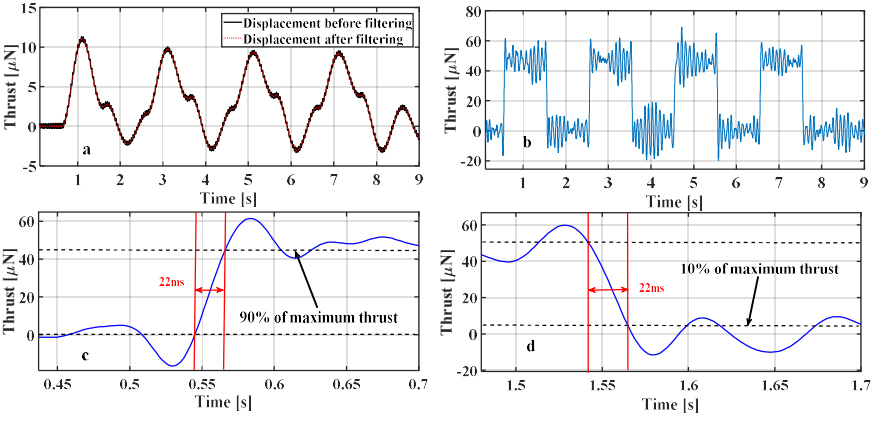

Fig. 7. Electromagnetic force response time measurement.

The response time of electromagnetic force is calibrated by the torsional pendulum in order to verify the limit response ability of the pendulum.

As shown in Fig. 2, the function generator outputs a square wave so as to energize the electromagnetic solenoid present in the torsional pendulum system. The electromagnetic force is generated between the electromagnetic solenoid and the permanent magnet. The electromagnetic force rise/fall time is then measured by the torsional pendulum. The result is as shown in Fig. 7.

It takes about 22 ms for the electromagnetic force measured by the torsional pendulum to rise to 90% of its maximum thrust. Similarly, it takes 22 ms for this force to drop from the maximum value to 10% of its maximum thrust, however, the actual electromagnetic force rise/fall time tends to be significantly lower than 22 ms, which indicates that the 50 μN thrust step measured within 22 ms happens to have reached the limit of torsional pendulum measurement. The manner in which the measurement limit of torsional pendulum can be improved is also discussed in Sec. 4.

3.3. *Thruster calibration*

In this study, a 6U satellite coldgas micro-thruster ground principle prototype was calibrated for parameters, such as thrust size, thrust noise and response time. The test results are as follows:

As shown in Fig. 8, if the thruster's working medium is air and the background vacuum is about 2×10^{-2} Pa, the measured thrust is equal to 222 μN and the flow is about 17.95 sccm. Hence, the specific impulse is calculated to be about 64 s.

The cold gas thruster noise performance evaluation is illustrated in Fig. 9. The thruster is operated under a constant measured thrust level of 222 μN. PSD levels of the thrust noise remain below 0.1 μN in the frequency range of 30 mHz–1 Hz.

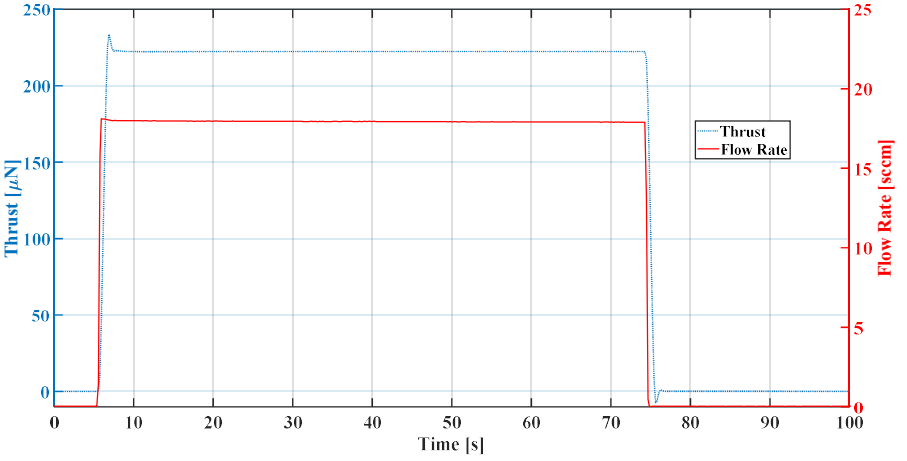

Fig. 8. (Color online) Calibration of thrust and flow. The blue dotted line represents thrust and the red solid line represents flow.

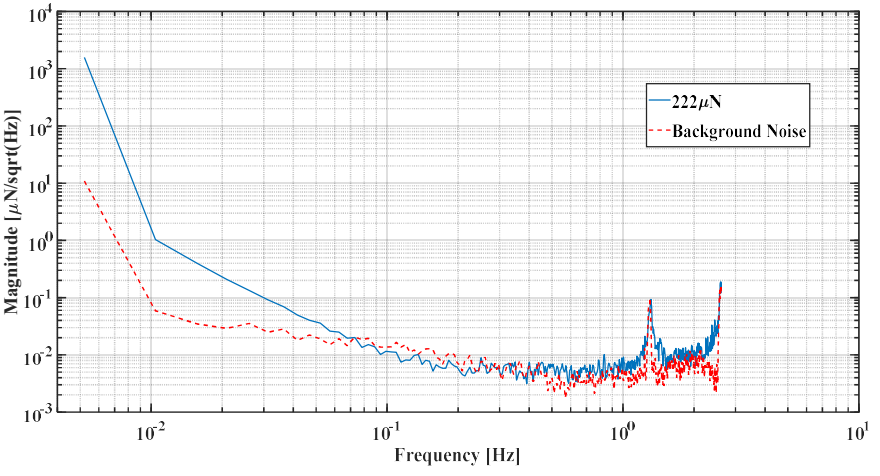

Fig. 9. (Color online) PSD of thrust noise with a thrust level of 222 μN (red dotted line). The solid blue line is PSD of thrust measurement system background noise.

Furthermore, the response time of the thruster is calibrated as well. The thruster performs with a 0.1 Hz square wave pulse. The measurement results are as shown in Fig. 10. The response time of cold gas thruster is exhibited in Fig. 10. Figure 10(a) demonstrates the displacement curve of the torsional pendulum, and Fig. 10(b) portrays the thrust curve reversed by the displacement curve. Considering the effect of delay in the measurement, the thrust rise time appears to be less than 23 ms, and the fall time tends to be less than 28 ms.

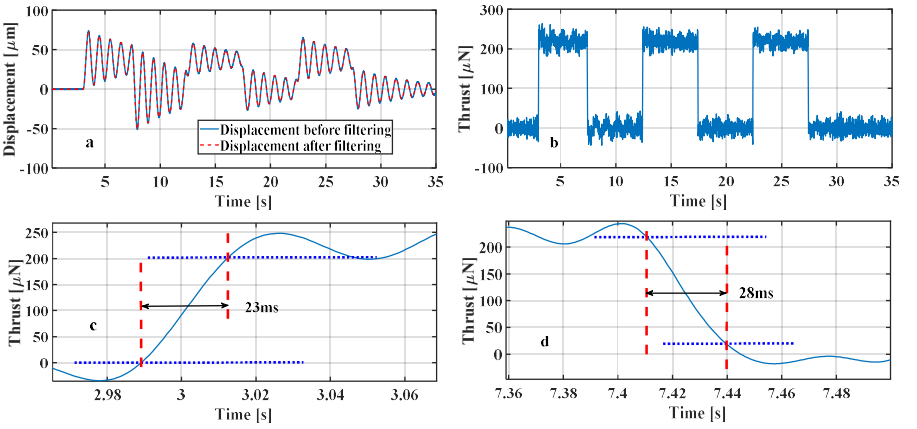

Fig. 10. Response time of cold gas thruster.

4. Discussion

A 10 ms delay exists between the measured and the actual response time, as highlighted in Sec. 3.1. A similar scenario is described in Sec. 3.2. Following these results, the source of the measurement delay is analyzed in Sec. 4.1. Improving the ability of the torsional pendulum to better measure the response time is discussed in Sec. 4.2.

4.1. *Discussionof the measurement delay*

Keeping in mind the convenience of calculation, over a short period of time, it can be considered that the thrust force is proportional to time during the thrust rise time period. The thrust acts on the torsional pendulum. The motion course of the torsional pendulum is a single degree of freedom with damped forced vibration. Its motion equation is as follows:

$$\begin{cases} j\ddot{x}+\lambda\dot{x}+kx=F(t)Lb \\ \qquad\qquad\qquad 0\le t\,, \\ x(0)=0,\ \dot{x}(0)=0 \end{cases} \tag{12}$$

Where

$$\begin{cases} F(t)=\delta t & 0\le t\le t_0 \\ F(t)=\delta t_0 & t_0\le t \end{cases}. \tag{13}$$

When $t \le t_0$, the analytical solution of the displacement is as follows:

$$x(t)=e^{-\zeta\omega_0 t}\left[\frac{2\zeta\delta Lb}{J\omega_0^3}\cos(\omega_d t)+\frac{\delta Lb(2\zeta^2-1)}{J\omega_0^2\omega_d}\sin(\omega_d t)\right]+\frac{\delta Lbt}{J\omega_0^2}-\frac{2\zeta\delta Lb}{J\omega_0^3}, \tag{14}$$

where ζ is the dimensionless parameter damping ratio and $\zeta = \lambda / (2\sqrt{kJ})$, $\omega_d = \omega_0\sqrt{1-\zeta^2}$, $\omega_0 = \sqrt{k/J}$.

Assuming the thrust to be about 50 μN and the rise time about 1 ms, the torsional pendulum system parameters are utilized to calculate x, while the damping effect is disregarded when $t = 0.001$ and $x = 0.062$ nm. To infer the thrust rise time, the sensor needs to measure about 0.062 nm within 1 ms. The displacement sensor employed in the experiment possesses a resolution of 1 nm during high-frequency measurement. Furthermore, high-frequency measurement results in displacement noise suppressing the 0.062 nm value displacement. When the displacement is subjected to low-pass filtering, the measurement delay surfaces.

Figure 11 displays the result of the numerical simulation after a thrust of magnitude 50 μN and a rise and fall time of 1 ms is applied to the torsional pendulum. Figure 11(a) illustrates the numerical simulation result when the resolution value is set to 10 nm, and Fig. 11(b) represents the numerical simulation result when the resolution value is set to 0.001 nm. Undertaking a comparison between a and b, the effective displacement signal emerges indistinguishable due to insufficient resolution. After executing dual differential noise amplification, the thrust step is seen to be completely suppressed. Figure 11(c) exhibits the result after filtering with a resolution of 10 nm. Very distinctive thrust steps appear after filtering. In Fig. 11(d), the thrust after filtering is compared with the real thrust, and an evident delay is witnessed post filtering.

If the dynamic thrust is inverted by the dynamic equation, the resolution of the displacement sensor appears insufficient, while the displacement noise generated during high-frequency measurement tends to be amplified by the first-order and second-order difference. The factual thrust steps tend to be completely concealed by noise, making it highly necessary to subject the displacement to a low-pass filtering process. However, the

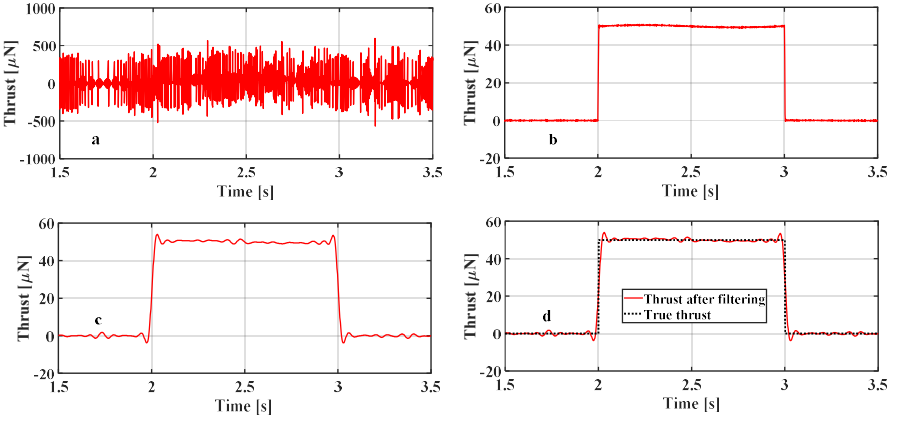

Fig. 11. Simulation results.

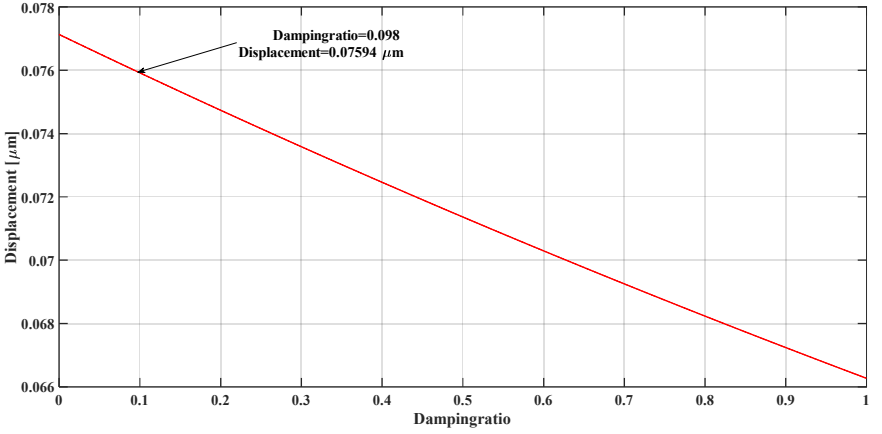

Fig. 12. Influence of damping ratio.When the damping ratio gradually increases, the displacement gradually decreases.

low-pass filtering process causes a delay in the response time of the torsional pendulum measurement. Therefore, it is vital to consider the displacement resolution ability of the displacement sensor under high-frequency measurement. On the one hand, the system demands a displacement sensor with higher resolution value. On the other hand, the system parameters can be suitably configured so as to amplify the displacement through the present model of the torsional pendulum.

4.2. *Discussion of system improvement*

Considering the response time index of "Taiji-1" and μRIT, suppose the thrust F to be about 25 μN and the corresponding rise time to be 50 ms. According to Eq. (14), the dimensionless parameter damping ratio is used as a variable. When f_0 is 1.015 Hz and J is 0.0053747 kg·m^2, calculate x at the 50th ms. The result is as shown in Fig. 12.

The lower the damping ratio of the torsional pendulum, the greater is the displacement, and the more beneficial it is for the measurement. The damping ratio of the system is about 0.098, and the displacement is about 1.5% smaller than the undamped case. It is evident from the above figure that the displacement loss is about 7% around the damping ratio of 0.5. A conservative estimate suggests that a damping ratio below 0.5 is acceptable and satisfactory.

Further, the influence on displacement is considered when J and f_0 are independent variables. For the convenience of calculation, assuming the damping ratio to be 0. The result is as shown in Fig. 13.

When the moment of inertia increases gradually, the displacement decreases rapidly. When the natural frequency increases gradually, the displacement decreases gradually. The spot pointed out by the arrow in the above-mentioned figure is the position at which

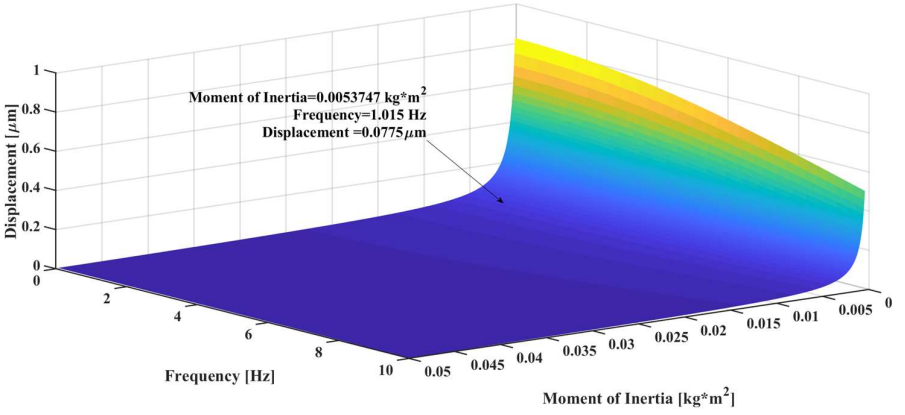

Fig. 13. Influence of moment of inertia and frequency.

the system parameter of the torsional pendulum is calculated, and the displacement is about 0.0775 μm, which is appreciably greater than the resolution of the sensor under high-frequency measurement. In addition, with the response time being 50 ms, it is not required to measure the displacement under a particularly high frequency, hence the resolution of the displacement stands further enhanced.

The damping and frequency of this system appears appropriate for the measurement. For future research, emphasis will be laid on reducing the mass or shortening the length of the torsional pendulum to achieve a reduction in the moment of inertia. In addition, during the functioning of the vacuum system, the high-frequency vibration produced by the mechanical and molecular pump also affects the measurement, hence, isolation of the measurement system from vibration is another vital aspect to be considered for attaining reasonable measurement. It is noteworthy that the above discussion is carried out under the impression that the mass of the thruster is not included in the measurement. The coldgas thruster mentioned in Sec. 3.3 weighs only 9 g, which can produce minimal effect on the torsional moment of inertia. However, a heavy thruster has the tendency to considerably increase the moment of inertia, which in turn will increase the measurement delay.

5. Conclusion

In response to the measurement requirements of the thrust response time regarding the micro-thruster on the "Taiji-1" technology test satellite of the gravitational wave detection "Taiji Program in Space", the dynamic equation of the torsional pendulum was established and then utilized to invert the characteristics of the dynamic thrust change with time by considering the torsional pendulum angular displacement, thereby measuring the rise/fall time of the thrust applied to the torsional pendulum. Finally, the following conclusions are drawn:

(1) The thrust measurement range of the system is about 0.025–400 μN, with the resolution touching 0.025 μN, and the background noise in the steady-state performs better than 0.1 μN/Hz$^{1/2}$ between 1 mHz–1 Hz.

(2) Based on the inversion of the torsional pendulum dynamic equation employed to measure the thrust rise/fall time, when the torsional pendulum remains unloaded, the thrust response time of the order of 10 ms can be measured for a thrust step in tens of micronewtons, which is a suitable criteria for measuring the thrust response time of the micro-thruster utilized in the "Taiji-1" technical test satellite.

This system has been successfully tested and applied to the engineering acceptance test of the "Taiji-1" technology test satellite drag-free radio-frequency ion micro-propulsion system and attitude control coldgas micro-propulsion system prototypes, identification parts and flight-model. Furthermore, the in-orbit calibration results of the micro-thruster show immense consistency with the torsion calibration results, paving a way for a fruitful series of space experiments.

Acknowledgments

This work is supported by the Strategic Priority Research Program of Chinese Academy of Sciences (Nos. XDB23030300 and XDA1502070901, XDA1502070503, XDA1502110105). Chao Yang and Jian-Wu He equally contribute to this work.

References

1. D. Reitze, The observation of gravitational waves from a binary black hole merger, in *APS Meeting*, APS Meeting Abstracts (Portland, Oregon, 2016), p. JA1.002.
2. Y. L. Wu, *Int. J. Mod. Phys. A* **33**, 1844014 (2018).
3. LISA Consortium. LISA: laser interferometer space antenna — aproposal in response to the ESA call for L3 mission concepts[EB/OL] (2019).
4. Z. R. Luo, M. Zhang, G. Jin *et al.*, *J. Deep Space Explor.* **7**, 3 (2020).
5. P. McNamara, S. Vitale and K. Danzmann, *LISA Pathfinder* (American Institute of Physics, 2006).
6. M. Armano, H. Audley, G. Auger *et al.*, *Phys. Rev. Lett.* **116**, 23 (2016).
7. D. Cyranoski, *Nature* **531**, 150 (2016).
8. W. R. Hu and Y. L. Wu, *Natl. Sci. Rev*. **4**, 685 (2017).
9. Chinese satellite tests space-based gravitational wave detection technologies, https://chinadaily.com.cn/a/201909/20/WS5d84cebaa310cf3e3556cac6.html.
10. J. W. He, P. Liu and R. L. Gao *et al.*, *Plasma Sci. Technol.* **22**, 6 (2020).
11. D. Packan, J. Bonnet and S. Rocca, Thrust measurements with the ONERA micronewton balance, *Int. Electric Propulsion Conf.*, *IEPC-2007-118* (Florence, Italy, 2007).
12. C. Stefano, M. Fabio, D. Filippo *et al.*, Nanobalance: The European balance for micro-propulsion, *Int. Electric Propulsion Conf.*, *IEPC-2009-182* (Michigan, USA, 2009).
13. J. Pérez Luna, C. H. Edwards, J. Gonzalez del Amo *et al.*, Development status of the ESA micro-Newton thrust balance, *Int. Electric Propulsion Conf.*, *IEPC-2011-011* (Wiesbaden, Germany, 2011).
14. M. Gamero-Castaño, *J. Propuls. Power* **20**, 736 (2004).
15. S. M. Merkowitz, P. G. Maghami, A. Sharma *et al.*, *Class. Quantum Grav.* **19**, 1745 (2002).

16. K. Jonathan, T. E. Porter and K. Michael, High precision thrust balance development at the George Washington, *Int. Electric Propulsion Conf.*, *IEPC-2017-405* (Georgia, USA, 2017).
17. Y. X. Yang, L. C. Tu, S. Q. Yang *et al.*, *Rev. Sci. Instrum.* **83**, 1 (2012).
18. W. J. Zhou, Y. J. Hong and H. Chang, *Rev. Sci. Instrum.* **84**, 407 (2013).
19. N. Davide, F. Pierre-Etienne, M. Fabio *et al.*, Direct thrust and thrust noise measurements on the LISA pathfinder field emission thruster, *Int. Electric Propulsion Conf.*, *IEPC-2009-183* (Michigan, USA, 2009).
20. O. Neunzig, C. Drobny and M. Tajmar, Development of a compact milli-newton thrust balance and characterization of a miniature hall-effect thruster, in *Int. Electric Propulsion Conf.*, *IEPC-2017-375* (Georgia, USA, 2017).
21. A. H. Yan, B. C. Appel and J. G. Gedrimas, MilliNewton thrust stand calibration using electrostatic fins, in *47th AIAA Aerospace Sciences Meeting including The New Horizons Forum and Aerospace Exposition*, *AIAA 2009-212* (Orlando, Florida).
22. R. Legtenberg, A. W. Groeneveld and M. Elwenspoek, *J. Micromech. Microeng.* **6**, 320 (1999).
23. C. Chen and C. Lee, *Sens. Actuators A, Phys.* **115**, 530 (2004).
24. C. Yang, J. W. He, Q. Kang *et al.*, *Chin. Opt.* **12**, 526 (2019).